A comparison of through-space population transfers from half-integer spin quadrupolar nuclei to 1H using MQ-HETCOR and MQ-SPAM-HETCOR under fast MAS.

A. Sasaki, Julien Trebosc, Jean-Paul Amoureux

ARTICLE

A comparison of through-space population transfers from half-integer spin quadrupolar nuclei to ^{1}H using MQ-HETCOR and MQ-SPAM-HETCOR under fast MAS

Received 00th January 20xx,
Accepted 00th January 20xx

DOI: 10.1039/x0xx00000x

Akiko Sasaki,[a] Julien Trébosc,[b] Jean-Paul Amoureux*[b,c,d]

In this article, we compare the various schemes of magnetization transfer from half-integer quadrupolar spins to ^{1}H nuclei and we establish an efficient protocol to perform these transfers under MQMAS high-resolution with the MQ-HETCOR and MQ-SPAM-HETCOR experiments under fast MAS. The MQMAS efficiencies are analyzed with SIMPSON simulations, and the CPMAS and RINEPT magnetization transfers are compared at 62.5 kHz MAS using {^{23}Na}-^{1}H and {^{27}Al}-^{1}H MQ-HETCOR and MQ-SPAM-HETCOR experiments performed on NaH_2PO4, Na_2HPO_4, Na citrate dihydrate and ipa-AlPO-14 powder samples. We discuss the pros and cons of these approaches, aiming to record 2D spectra of the best possible quality under fast MAS. We also incorporate some experimental approaches to reduce the total experiment time of such long 2D experiments.

Key words: solid-state NMR, HETCOR, quadrupolar nuclei, MQMAS, SPAM, fast MAS.

I. Introduction

During the last decade, several schemes to acquire HETCOR (hetero-nuclear correlation) two-dimensional (2D) spectra between spin-1/2 and half-integer spin quadrupolar nuclei have been proposed in ssNMR (solid-state nuclear magnetic resonance). All these sequences use magic angle spinning (MAS) of the sample to enhance the resolution.

The HETCOR sequence may start from the quadrupolar nucleus to profit of its often-small longitudinal relaxation time, hence allowing using short recycling delays (RD). In the reverse way, the sequence starts from the spin-1/2 nucleus to profit of its often-large magnetization. The choice between the two variants depends on the ratios between the Larmor frequencies, the natural abundances, the longitudinal relaxation times, and the linewidths of the two nuclei. It must be reminded here that the linewidth of the quadrupolar nucleus corresponds to its central-transition (CT), between the ±1/2 Zeeman levels, which is broadened by the anisotropic second-order quadrupole interaction.

When an isotropic dimension is desired for the quadrupolar nucleus, a high-resolution 2D method, such as MQMAS (multiple-quantum MAS)[1] or STMAS (satellite-transition MAS),[2] has to be employed. In this case, the HETCOR sequence becomes a 3D experiment if it starts from the spin-1/2 nucleus,[3] whereas it remains a 2D one in the reverse way. As a result, mostly the second type of 2D HETCOR sequences have been used presently to shorten the experiment time, T_{exp}, and they were successfully demonstrated for several pairs of nuclei such as {^{27}Al}-^{31}P, {^{27}Al}-^{27}Si and {^{23}Na}-^{31}P. These high-resolution HETCOR experiments utilize an MQMAS or STMAS quadrupolar filter followed with either one population transfer done with CPMAS (MQ-CP-HETCOR[4–10] or ST-CP-HETCOR[11]), RINEPT (MQ-J-RINEPT[10,12–15] or MQ-D-RINEPT[13,16–18]), or two consecutive transfers with the MQ-J-HMQC[3] or HMQC-ST[19] experiments. These methods have been further combined with the SPAM sensitivity enhancement scheme (SPAM-MQ-HETCOR).[10,13,14,16]

For the through-space HETCOR experiments, which rely on the hetero-nuclear dipolar interactions between spin-1/2 and half-integer spin quadrupolar nuclei, the CPMAS transfer is often considered difficult and time-consuming, especially in the case of small S/N, as it requires a careful optimization of multiple parameters. On the contrary, the RINEPT approach is claimed to be robust to offset and rf-inhomogeneity (and hence relatively easier to set up) and more efficient than the PRESTO approach[20] under fast MAS.[21,22]

Recently, owing to the technical development of fast MAS probes and small-diameter rotors, higher spinning rates have become more and more accessible on an everyday basis. This is especially important for ^{1}H-detected HETCOR experiments involving quadrupolar nuclei,[4,16,17,19,23–27] because the higher

[a] Bruker Japan K.K., 3-9, Moriya-cho, Kanagawa-ku, Yokohama-shi, Kanagawa 221-0022, Japan.
[b] Univ. Lille, CNRS, Centrale Lille, ENSCL, Univ. Artois, UMR 8181 – UCCS – Unit of Catalysis and Chemistry of Solids, F-59000 Lille, France.
[c] Bruker Biospin, 34 rue de l'industrie, F-67166 Wissembourg, France.
[d] RIKEN RSC NMR Science and Development Division, 1-7-22 Suehiro-cho, Tsurumi-ku, Yokohama-shi, Kanagawa, 230-0045, Japan.

Electronic Supplementary Information (ESI) available. See DOI: 10.1039/x0xx00000x

^{1}H resolution under fast MAS makes it a more practically promising approach in ssNMR investigations.

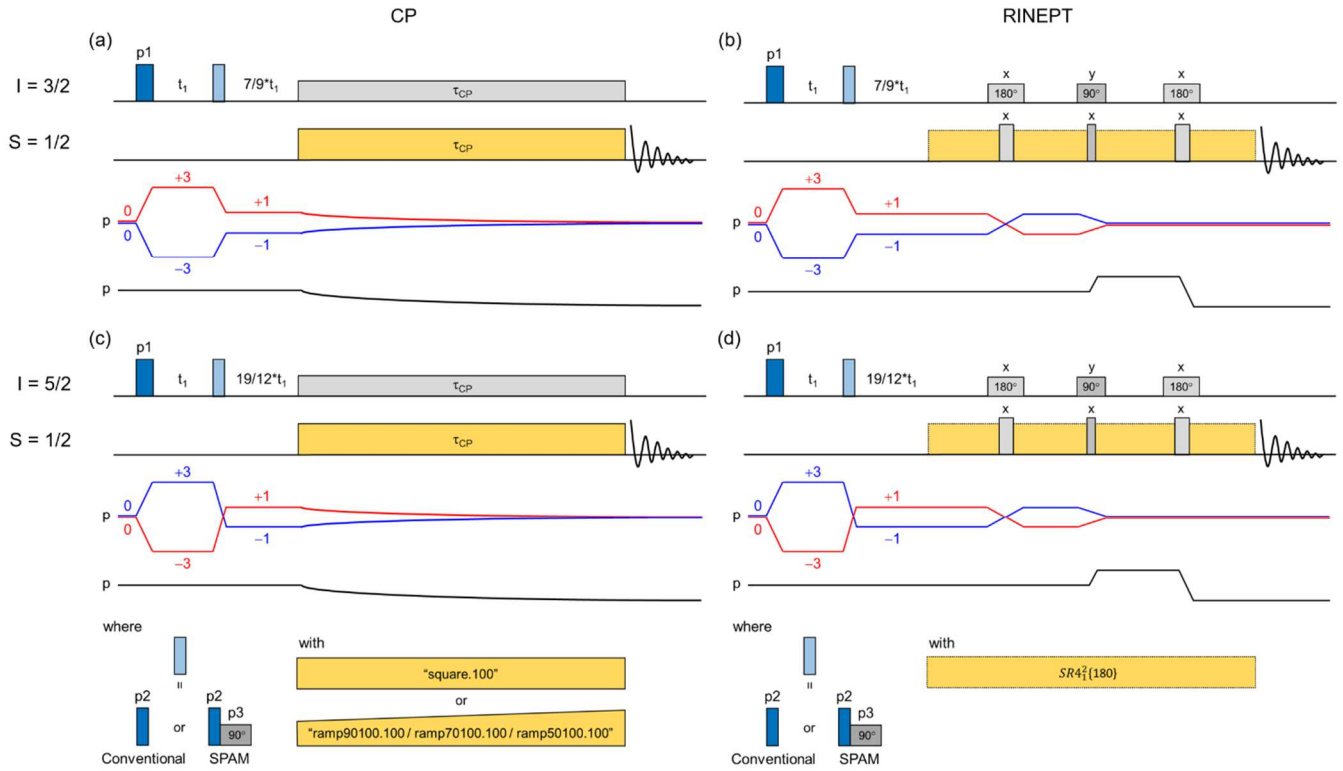

Fig.1 Pulse sequences and coherence transfer pathways of (a,b) {^{23}Na}-^{1}H and (c,d) {^{27}Al}-^{1}H MQ-HETCOR and MQ-SPAM-HETCOR experiments via population transfer by (a,c) CP and (b,d) RINEPT used in the following investigations.

In this article, we employ two dipolar-mediated spin-systems, ^{23}Na-^{1}H and ^{27}Al-^{1}H, and utilize the sensitivity advantage of the ^{1}H detection under fast MAS in high-resolution 2D quadrupolar HETCOR experiments. We focus on the MQMAS quadrupolar filter and perform a comparison of the currently available population transfer schemes using MQ-HETCOR and MQ-SPAM-HETCOR 2D spectra. Fig.1 summarizes the pulse sequences and coherence transfer pathways used in the following investigations: (a,b) {^{23}Na}-^{1}H and (c,d) {^{27}Al}-^{1}H MQ-HETCOR and MQ-SPAM-HETCOR experiments via (a,c) CPMAS and (b,d) RINEPT. It should be reminded here that the split-t_1 approach[28] that has been employed in MQMAS experiments is inherent to the MQ-HETCOR sequences used in this article. We demonstrate a step-by-step experimental protocol to set up efficiently the CPMAS, RINEPT and SPAM blocks with the aid of a series of 1D acquisitions and of simulations. This protocol is practically important upon acquisition of time-consuming 2D quadrupolar HETCOR spectra with the best possible quality for a given (and often limited) amount of spectrometer time. We discuss the pros and cons of these high-resolution quadrupolar HETCOR approaches under fast MAS conditions. We conclude by introducing two experimental approaches to reduce the total experiment time of such long 2D experiments.

II. Methods

All experiments were performed using a Bruker Avance NEO spectrometer with a B_0 = 14.1 T wide-bore magnet at Larmor frequencies of 158.8 (^{23}Na), 156.5 (^{27}Al) and 600.3 (^{1}H) MHz, equipped with a 1.3 mm HX MAS probe. The maximum rf field strengths of ν_1 = 145 (^{23}Na), 150 (^{27}Al) and 155 (^{1}H) kHz were attainable. The spinning stability was maintained by a MAS III unit within ± 10 Hz at ν_R = 20 and 62.5 kHz. The powder samples of NaH_2PO_4, Na_2HPO_4, sodium citrate dihydrate (Wako) were packed as purchased, and ipa-AlPO-14 was packed as synthesized. The chemical shifts were referenced using the sample itself as a secondary reference. The indirect dimensions of the 2D HETCOR spectra were referenced according to the unified representation.[29] The 4.0.6 version of the Topspin software was used throughout. We provide in the SI our TopSpin pulse sequences for MQ-HETCOR and MQ-SPAM-HETCOR experiments.

All MQMAS simulations were performed using the SIMPSON program.[30] The input parameters were the nucleus of interest (^{23}Na or ^{27}Al), spinning frequency (ν_R), rf-field strength (ν_1) and the quadrupolar coupling constant (C_Q). The quadrupole interaction, with η_Q = 0, was taken into account up to the second-order, without scalar or dipolar coupling. The powder averaging parameters (crystal file, number of γ-angles and maximum time step, Δt, over which the Hamiltonian is considered time independent) were tested for convergence, and a combination of ZCW20 × 10 γ-angles with Δt = 0.1 μs was sufficient for the given range of C_Q values used in the plot. Since the imaginary part of the signal was found to be minor,

only the real part of the signal is plotted as the signal intensity. Further computational details are given in the figure captions.

III. Setting up the experiments

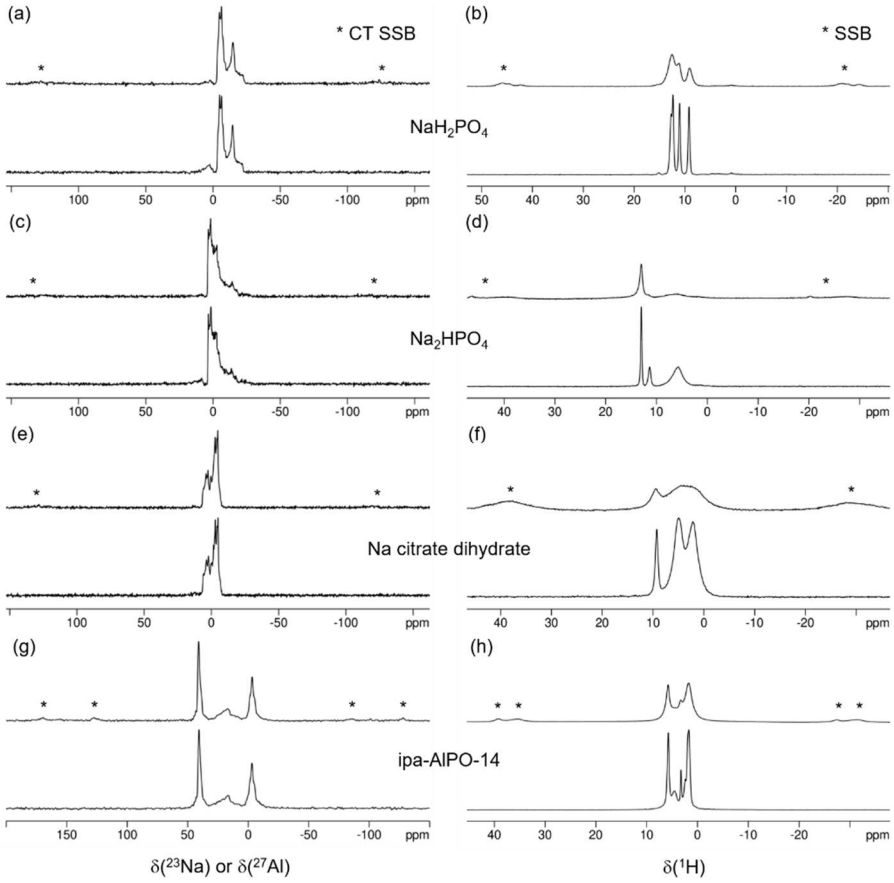

Fig.2 Examples of 1D (a,c,e) ^{23}Na, (g) ^{27}Al and (b,d,f,h) ^{1}H MAS spectra at ν_R = 20 kHz (top) and 62.5 kHz (bottom) of (a,b) NaH_2PO_4, (c,d) Na_2HPO_4, (e,f) Na citrate dihydrate and (g,h) ipa-AlPO-14, respectively.

Fig.**2** shows a series of ^{23}Na, ^{27}Al and ^{1}H 1D MAS spectra at ν_R = 20 and 62.5 kHz, of each of the four compounds used in the following HETCOR investigations: (a,b) NaH_2PO_4, (c,d) Na_2HPO_4, (e,f) sodium citrate dihydrate and (g,f) ipa-AlPO-14. Upon comparison of the spectra recorded at ν_R = 20 and 62.5 kHz, there is no apparent change for the second-order broadened ^{23}Na and ^{27}Al quadrupolar lineshapes, except for the presence/absence of small spinning sidebands. On the contrary, the ^{1}H MAS spectra of all four samples present significant changes in intensity and appearance at the two spinning frequencies. The increased resolution under fast MAS has a potential to obtain structural information that could not be detected at ν_R = 20 kHz. In this study, we make use of the ^{1}H resolution advantage under fast MAS to perform high-resolution quadrupolar HETCOR experiments with the ^{1}H detection in the direct dimension and isotropic ^{23}Na or ^{27}Al information in the indirect dimension.

Upon acquisition of 2D quadrupolar HETCOR experiments, which often lasts for a few hours or days, it is highly recommended to first establish the optimum conditions to acquire the 2D spectra with the best possible quality for the given experimental conditions (e.g. nature of the sample, quality of the probe, achievable spinning rate, amount of spectrometer time available etc.). We first describe the step-by-step protocol to set up the CPMAS, RINEPT and SPAM blocks as efficiently as possible, with the aid of prior insights for the MQMAS part provided by SIMPSON simulations followed by a series of 1D MAS acquisition. Fig.**S1** schematically describes the step-by-step procedures to set up the CPMAS and RINEPT transfers, with a series of 1D acquisitions that are recommended to carry out prior to any 2D acquisition. In the following paragraphs, we review the principles of CPMAS and RINEPT schemes from a practical point of view, and we give a brief description of the significance of each step for the sake of establishing an efficient experimental protocol upon successful acquisition of the 2D MQ-HETCOR spectra.

III.1. Setting up CPMAS

CPMAS transfers involving at least one quadrupolar nucleus are often considered as a challenge due to the very complex spin dynamics involved in both the spin-locking of the

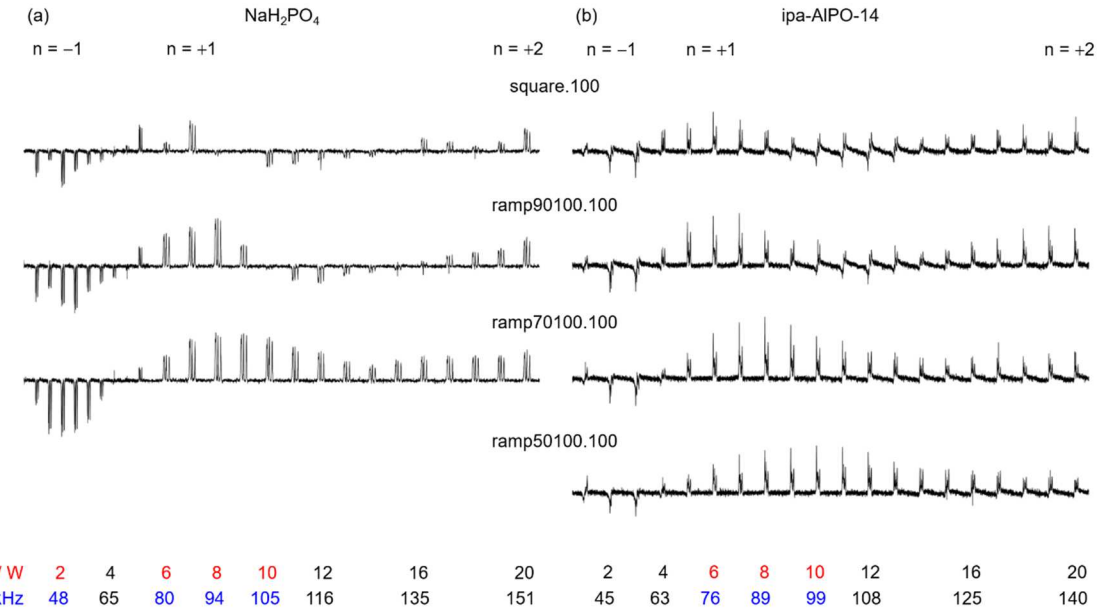

Fig.3 Examples of 1D (a) {^{23}Na}-^{1}H and (b) {^{27}Al}-^{1}H CPMAS profile versus the ^{1}H rf-field strength ($\nu_{1,H}$) of the contact pulse at ν_R = 62.5 kHz. The CP pulse sequence and the corresponding parameters are described in Fig.**S1**. (a) NaH_2PO_4: NS = 8, RD = 3 s, T_{exp} = 24 s each, τ_{CP} = 4 ms, $\nu_{1,Na}$ = 11 kHz. (b) ipa-AlPO-14: NS = 8, RD = 1 s, T_{exp} = 8 s each, τ_{CP} = 3.5 ms, $\nu_{1,Al}$ = 4.5 kHz. In blue ($\nu_{1,H}$) and red (W), we emphasize the efficient regions of CPMAS transfers.

quadrupolar magnetization and its transfer to the other nucleus. The quadrupolar CPMAS efficiency depends on several parameters such as: the rf-fields ($\nu_{1,H}$ for ^{1}H and $\nu_{1,I}$ for the quadrupolar nucleus, I), the spinning rate (ν_R), the offset, the quadrupole interaction described with $\nu_Q = 3C_Q/(2I(2I-1))$, and the magnitude of the ^{1}H-I dipolar interactions.[31,32] The spin-locking of the quadrupolar nucleus is characterized by the adiabaticity parameter, $\alpha = \nu_{1,I}^2/\nu_Q\nu_R$, and it is efficient only when either $\alpha >> 1$ (adiabatic passage) or $\alpha << 1$ (sudden passage). Under fast MAS (e.g. ν_R = 62.5 kHz), the $\alpha << 1$ condition is the only practical possibility, and it leads to low $\nu_{1,I}$ rf-fields of a few kHz. Under this spin-locking condition for the central-transition (CT), the CPMAS transfers between the two nuclei occur under the modified Hartmann-Hahn condition, $\nu_{1,H} = (I + 1/2)\nu_{1,I} + n\nu_R$, where I = 3/2, 5/2 etc. and typically n = ±1.

As an example, Fig.**3** shows some examples of 1D ^{23}Na→^{1}H and ^{27}Al→^{1}H CPMAS profiles of NaH_2PO_4 and ipa-AlPO-14 at ν_R = 62.5 kHz upon varying $\nu_{1,H}$ between 40 and 150 kHz. We should emphasize that these profiles are upon ^{1}H detection, and that the intensities strongly depend on varying $\nu_{1,H}$ by as small as 5-10 kHz, because the ^{1}H spectra only spread over 5-10 kHz (Fig.**2b**,**d**,**f**,**h**). It can also be observed that, upon quadrupolar CPMAS, the ramp shaped pulses perform better than the conventional square pulses, as often observed with spin-1/2 systems. For a given sample, optimizing the contact time (τ_{CP}) is also a prerequisite, as with spin-1/2 systems. For the sake of sensitivity, a long value, $\tau_{CP} \approx$ 3-4 ms, may be used to start the optimization. We should particularly note that the quadrupolar CPMAS transfer is very sensitive to the offset in the quadrupolar channel due to the use of low rf-field. Since the CPMAS transfers depend on the C_Q value, two sites with very different C_Q values may not necessarily be observable simultaneously under the same CPMAS conditions. In this case, they may require separate sets of optimization parameters, and hence several 2D acquisitions. For more 'molecular' systems, such as Na citrate dihydrate and ipa-AlPO-14, both the spin-locking and the CPMAS transfer efficiencies may decrease due to the presence of dynamics (e.g. water molecules swapping positions or template molecules freely moving etc.). In this case, the CPMAS intensity may be low, necessitating the use of an increased number of scans (NS) to achieve an acceptable S/N (compare in Fig.**3** the S/N of NaH_2PO_4 and ipa-AlPO-14).

In short, for a successful observation of quadrupolar CPMAS spectra under fast MAS, we recommend the use of a low rf-field on the quadrupolar channel (a few kHz) and a long contact time (τ_{CP} = 3-4 ms) for the sake of efficient spin-locking and increased sensitivity, respectively. The CPMAS transfers hence require 4 main parameters to be optimized: the contact time (τ_{CP}), the two rf-fields ($\nu_{1,H}$ and $\nu_{1,I}$) and the offset, especially on the quadrupolar channel.

III.2. Setting up RINEPT

To circumvent the complicated setting problems associated with the quadrupolar CPMAS, the D-RINEPT (dipolar-mediated refocused insensitive nuclei enhanced by polarization transfer) approach has been implemented to acquire 2D HETCOR spectra between ^{1}H and half-integer spin quadrupolar nuclei,

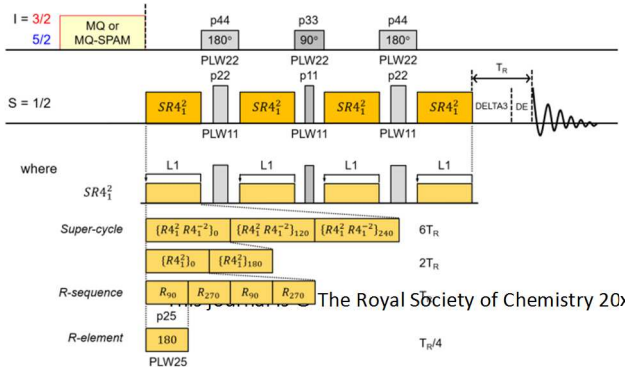

Fig.4 Schematic illustration of the $SR4_1^2$ (180) recoupling scheme used in this study.

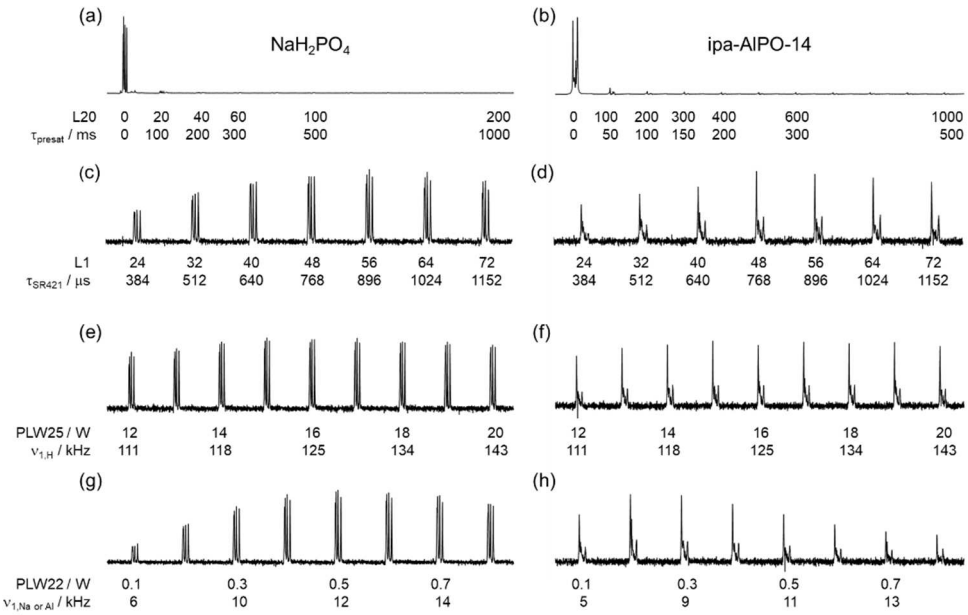

Fig.5 $^{23}Na \rightarrow {}^{1}H$ (left) and $^{27}Al \rightarrow {}^{1}H$ (right) RINEPT profiles at ν_R = 62.5 kHz with $SR4_1^2$ (180) recoupling upon varying (a,b) the ^{1}H presaturation period (τ_{presat}), (c,d) the recoupling period (τ_{SR421}), (e,f) ^{1}H rf-field strength ($\nu_{1,H}$) and (g,h) ^{23}Na or ^{27}Al rf-field strength ($\nu_{1,Na}$ or $\nu_{1,Al}$). The RINEPT pulse sequence and the corresponding parameters are described in Fig.4 and Fig.**S1**. (a,c,e,g) NaH_2PO_4: d20 = 5 ms, (a) NS = 1, RD = 3 s, T_{exp} = 3 s each, (c,e,g) NS = 16, RD = 1 s, T_{exp} = 24 s each. (b,d,f,h) ipa-AlPO-14: d20 = 500 µs, (b) NS = 1, RD = 1 s, T_{exp} = 1 s each, (d,f,h) NS = 16, RD = 1 s, T_{exp} = 21 s each.

such as ^{23}Na, ^{27}Al, ^{17}O and ^{35}Cl.[4,16,17,19,23–25,27] The hetero-nuclear coupling is typically reintroduced using the symmetry-based $SR4_1^2$ scheme.[33] Fig.**4** shows a schematic illustration of the D-RINEPT sequence with this $SR4_1^2$ scheme, shortened to RINEPT hereafter. Using a rectangular π-pulse as basic element, the sequence $R4_1^2 = 180_{90}180_{270}180_{90}180_{270}$, which lasts one rotor period ($T_R = 1/\nu_R$), is super-cycled to $[R4^2{}_1R4^{-2}{}_1]_0[R4^2{}_1R4^{-2}{}_1]_{120}\,[R4^2{}_1R4^{-2}{}_1]_{240}$, and the ^{1}H irradiation is applied with $\nu_{1,H} = 2\nu_R$ = 125 kHz at ν_R = 62.5 kHz. This sequence suppresses the ^{1}H isotropic chemical shifts, the hetero-nuclear J-couplings and ^{1}H-^{1}H dipolar couplings to the first-order.[21] The three pulses on the quadrupolar channel are CT-selective with a low rf-field of a few kHz, and their durations have been fixed in this study at 8 (T_R/2) and 16 µs (T_R), for the π/2 and π-pulses, respectively.

Fig.**5** presents the 1D $^{23}Na \rightarrow {}^{1}H$ and $^{27}Al \rightarrow {}^{1}H$ RINEPT-HETCOR profiles at ν_R = 62.5 kHz and the $SR4_1^2$ recoupling with respect to the ^{1}H recoupling period (τ_{SR421}) and the ^{1}H, ^{23}Na or ^{27}Al power inputs, using NaH_2PO_4 and ipa-AlPO-14. Due to the possible direct excitation of the ^{1}H magnetization by the recoupling pulses, the 2D spectra may suffer from artefacts. This is especially the case for samples with long $T_{1,H}$ values (e.g. > 100s in NaH_2PO_4, Na_2HPO_4 and sodium citrate dehydrate). These artefacts can be avoided by applying during τ_{presat} a ^{1}H pre-saturation pulse train prior to the MQ excitation, and it results in a slightly longer experiment time than the CPMAS equivalent (see section IV for the comparison of spectra).

The recoupling period can be optimized experimentally starting from the relation, $\tau_{SR421} \approx 9.44/(2b_{HI})$, where b_{HI} is the dipolar coupling constant in rad/s.[20] For example, for NaH_2PO_4, the optimum value, $\tau_{SR421} \approx$ 768-1024 µs, corresponds to a Na-H dipolar coupling of 0.7-1.0 kHz, in good agreement with the value estimated from the crystal structure.[34] The intensity is very robust with respect to $\nu_{1,H}$ around its theoretical value of $2\nu_R$ (Fig.**5e,f**). It is more sensitive to the quadrupolar rf-field (Fig.**5g,h**), but less than with CPMAS (Fig.**3**).

To summarize, the RINEPT transfer only requires one main parameter to optimize, the recoupling time (τ_{SR421}). This makes the RINEPT setting much easier than that for CPMAS, especially in the case of small S/N ratios.

III.3. Setting up SPAM

Despite of the previous optimum conditions for CPMAS or RINEPT, the signal intensity of MQ-HETCOR experiments may still be low to be useful in ssNMR applications, compared to other experiments used on an everyday basis. One way to enhance the S/N of the MQ-HETCOR spectra is to incorporate the SPAM (soft-pulse added mixing) approach that increases the efficiency of the MQ conversion.[35,36] Among other equivalent schemes, such as FAM,[37] DFS[38] and HS,[39] which have been successfully demonstrated for the excitation and conversion of the MQ coherences, here we employ the conversion of the MQ coherences by SPAM, which is advantageous in that no complicated optimization process is required and hence is easy to set up. Upon SPAM, the MQ conversion hard-pulse (HP) is replaced with a composite pulse (Fig.**1** bottom). This means a HP immediately followed with a CT-selective π/2-pulse with a proper phase depending on the selected coherence pathway. Previously, we have demonstrated the successful implementa-tion of SPAM-MQMAS under fast MAS conditions.[40] In the following, we describe the equivalent set of procedure for MQ-SPAM-HETCOR implementation, with the aid of SIMPSON simulations and acquisition of 1D spectra.

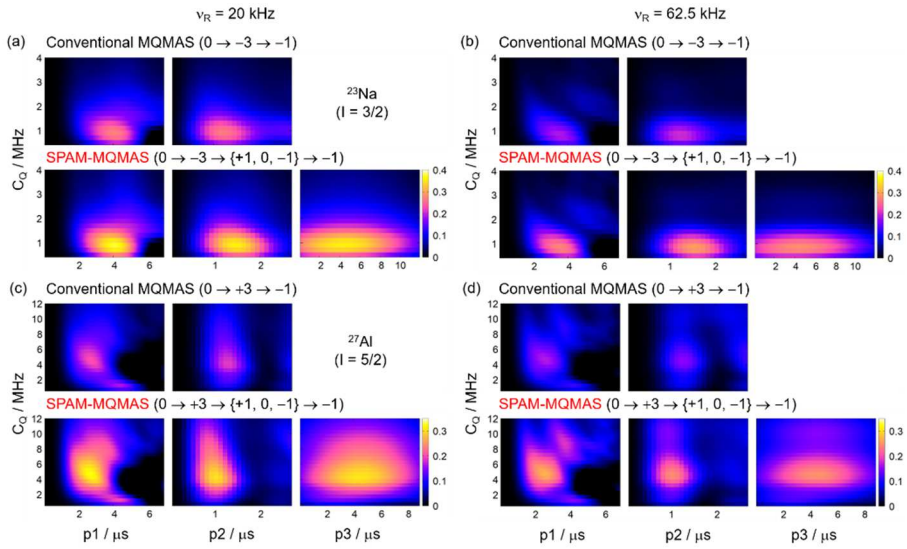

Fig.6 Simulated signal intensity for (a,b) ^{23}Na and (c,d) ^{27}Al MQMAS with respect to each pulse length (p1, p2 and p3) for a range of C_Q values at B_0 = 14.1 T with ν_1 {p1, p2, p3} = {150, 150, 20} kHz, and ν_R = 20 (a,c) or 62.5 (b,d) kHz. For each plot, one of the pulse lengths (denoted in the x-axis) is varied while others are fixed. The combination of pulse lengths used within each plot is, for example, {p1, p2, p3} = {3.5, 1.0 (Conventional) /1.3 (SPAM), 6.0} or {3.0, 1.2 (Conventional) / 0.9 (SPAM), 4.0} μs, for ^{23}Na or ^{27}Al, respectively.

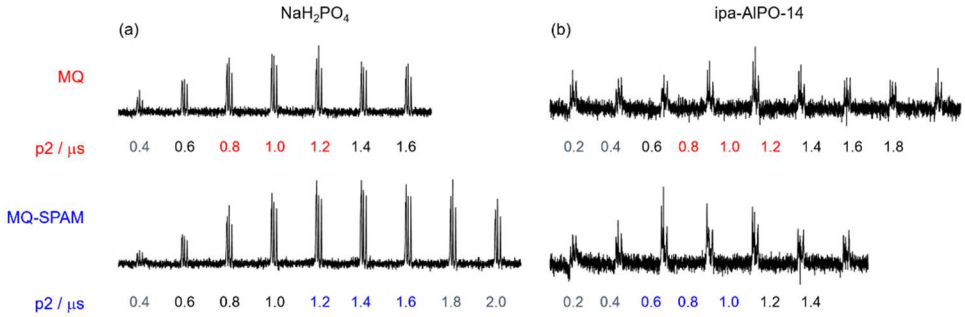

Fig.7 Examples of 1D (a) {^{23}Na}-^{1}H and (b) {^{27}Al}-^{1}H MQ-CP-HETCOR and MQ-SPAM-CP-HETCOR profiles versus the p2 pulse length at ν_R = 62.5 kHz and NS = 24. RD = 3/1 s, T_{exp} = 1.2/0.5 min each, MQMAS: {p1, p3} = {3, 6}/{2.5, 3.5} μs, CP: τ_{CP} = 4/3.5 ms, $\nu_{1,Na/Al}$ = 11/4.5 kHz, $\nu_{1,H}$ (ramp90100.100) = 52/89 kHz, for NaH_2PO_4/ ipa-AlPO-14, respectively.

Fig.**6** shows the simulated MQMAS intensity for I = 3/2 (a,b) or 5/2 (c,d) with conventional HP or SPAM conversion with respect to each pulse length (p1, p2 and p3) for a range of C_Q values at ν_R = 20 (a,c) and 62.5 (b,d) kHz. This signal is used for {^{23}Na}-^{1}H and {^{27}Al}-^{1}H MQ-HETCOR and MQ-SPAM-HETCOR experiments. In relation to the step of the selected coherence pathway for p2, $\Delta p = \pm 2$ or ± 4 (Fig.**1**), the SPAM phase condition is $\phi_3 = -\phi_2$ or $+\phi_2$, for I = 3/2 or 5/2, respectively.

Although fast MAS is a prerequisite for the ^{1}H resolution (Fig.**2**), the MQMAS efficiency decreases under fast MAS (compare the left and right plots in Fig.**6**).[41] On the contrary, it has been shown that, due to the decrease of the rotor period, the STMAS efficiency increases with the MAS frequency.[39] However, this MQMAS efficiency loss is overcome by the SPAM sensitivity enhancement. Theoretically, compared to MQ-HETCOR, the MQ-SPAM-HETCOR approach gives rise to a signal enhancement of 1.4 for I = 3/2 (^{23}Na) and 1.7 for I = 5/2 (^{27}Al).[10] These gains are confirmed by the intensity plots in Fig.**6**, and the application of SPAM at ν_R = 62.5 kHz gives a larger efficiency than that at ν_R = 20 kHz with conventional pulses.

We note (i) that the first pulse length (p1) is identical, irrespective of the presence or absence of SPAM, but (ii) that the optimum second pulse length (p2) is different between MQMAS and MQMAS-SPAM, due to the difference of the selected coherence pathways. Indeed, without SPAM, only one pathway is selected (-3 → -1 or +3 → -1), but with SPAM, all other available coherence pathways are mixed to add up. The simulations show that the overall signal intensity of both MQ-HETCOR and MQ-SPAM-HETCOR is sensitive to the p2 pulse length by a few tenths of μs. This was confirmed experimentally at ν_R = 62.5 kHz, by the {^{23}Na}-^{1}H and {^{27}Al}-^{1}H MQ-CP-HETCOR and MQ-SPAM-CP-HETCOR 1D profiles upon varying the p2 length between 0.2 and 2.0 μs by step of 0.2 μs (Fig.**7**). For I = 3/2, the optimum p2 length is longer with than without SPAM, whereas the opposite is true for I = 5/2.

For the sake of sensitivity, we recommend utilizing the SPAM approach to circumvent the inevitable MQMAS efficiency loss under fast MAS, and we suggest carefully optimizing the MQ conversion hard-pulse length (p2) upon acquisition of both MQ- and MQ-SPAM-HETCOR spectra, in accordance with the simulations (Fig.**6**) and the experiments

(Fig.7). This is utilized in the next section where we compare the series of MQ- and MQ-SPAM-HETCOR spectra.

IV. Comparison of 1D and 2D MQ- and MQ-SPAM-HETCOR spectra

Having established the optimum experimental conditions, we compare the 1D and 2D MQ-HETCOR spectra of the four selected compounds, recorded with CPMAS or RINEPT transfer and with or without SPAM conversion pulse.

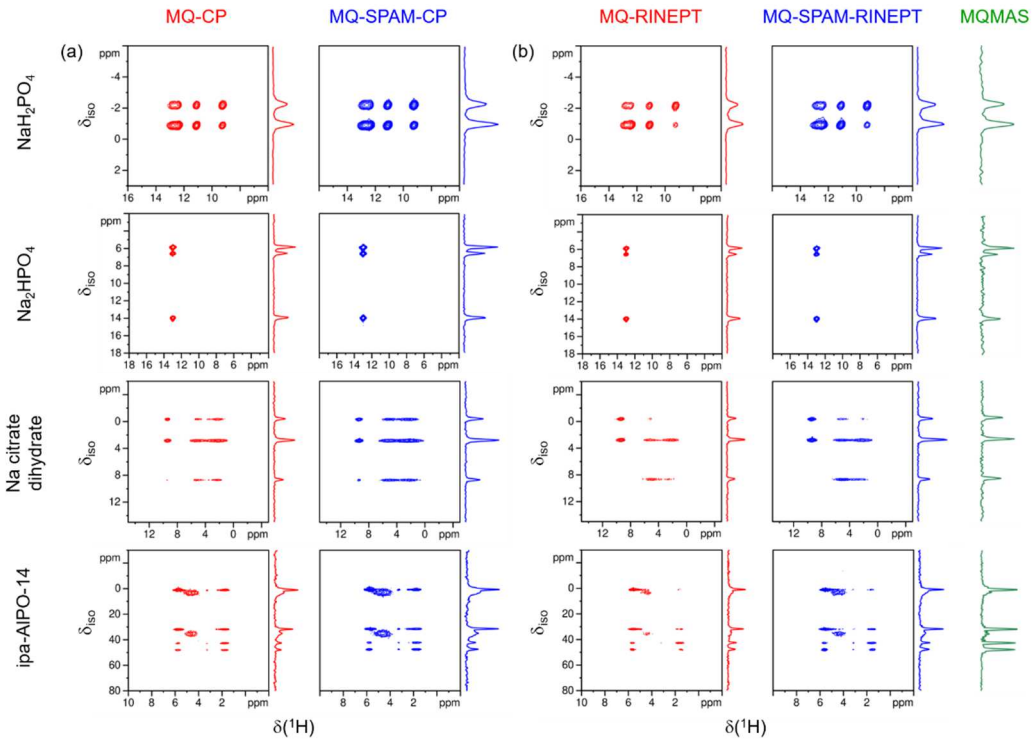

Fig.9 Examples of (a,b) {^{23}Na}-^{1}H and (c,d) {^{27}Al}-^{1}H MQ-HETCOR and MQ-SPAM-HETCOR 2D spectra at ν_R = 62.5 kHz via (a,c) CP and (b,d) RINEPT plotted with an expansion around the signal region. An isotropic projection of the 2D MQMAS spectra is shown for comparison. NS = 24/24/48/96, RD = 1/1/1/0.6 s, 600/800/600/500 t_1 increments, T_{exp} = 4-6/5.5-8/8-12/8.3-12.2 h each, for NaH_2PO_4/Na_2HPO_4/sodium citrate dihydrate/ipa-AlPO-14, respectively

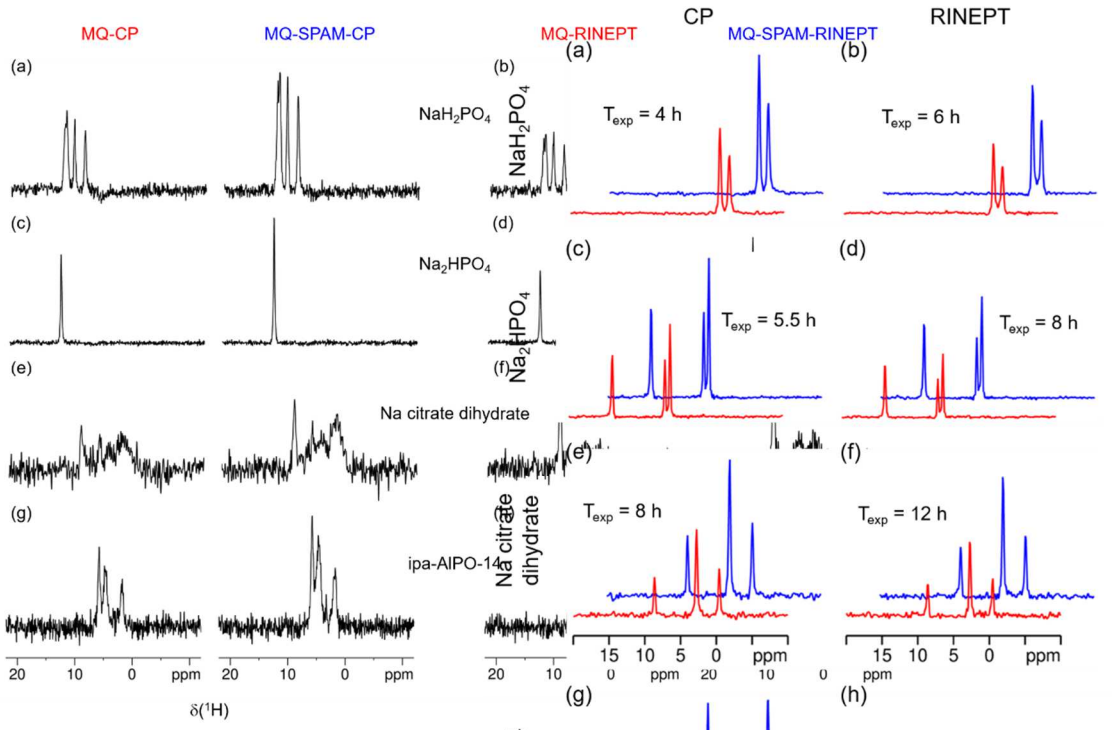

Fig.8 Comparison of 1D (a-f) {^{23}Na}-^{1}H and (g,h) {^{27}Al}-^{1}H MQ-HETCOR and MQ-SPAM-RINEPT of (a,b) NaH_2PO_4, (c,d) Na_2HPO_4, (e,f) Na citrate dihydrate and (g,h) ipa-AlPO-14.

IV.1. 1D MQ- and MQ-SPAM-HETCOR spectra

The 1D spectra correspond to the first FIDs of the 2D acquisitions (t_1 = 0). Since the signal intensities of these FIDs are proportional to the integrated intensities of the 2D spectra, they provide a quick preliminary insight to the success of the following 2D acquisitions, which often last for a few hours or days.

Fig.**8** shows the ^{23}Na→^{1}H and ^{27}Al→^{1}H MQ-HETCOR and MQ-SPAM-HETCOR 1D spectra at ν_R = 62.5 kHz, with CPMAS or RINEPT transfer, for each of the four samples. The use of the SPAM pulse is expected to give a signal gain of 1.4 or 1.7, for I = 3/2 (^{23}Na) or 5/2 (^{27}Al), respectively,[10] and this was observed experimentally upon comparison of the MQ-HETCOR and MQ-SPAM-HETCOR 1D spectra. Indeed, the SPAM gains with CPMAS and RINEPT were found to be 1.5 and 1.4 (NaH_2PO_4), 1.4 and 1.4 (Na_2HPO_4), 1.5 and 1.5 (sodium citrate dehydrate) and 1.5 and 1.6 (ipa-AlPO-14). It should be remembered that the total experiment time (T_{exp}) of RINEPT might be slightly longer than the CPMAS equivalent due to the presence of the ^{1}H saturation period. Here, the quadrupolar CPMAS efficiency was slightly higher than that of RINEPT (Fig.**8**). This is due to the efficient spin-locking under fast MAS, because the sudden passage condition, $\alpha = \nu_1^2/\nu_Q\nu_R << 1$, is then favourably satisfied. However, the experimental setting up with CPMAS may be much longer than with RINEPT, due to the four parameters to optimize, instead of a single parameter in the latter case.

IV.2. 2D MQ- and MQ-SPAM-HETCOR spectra

Fig.10 Comparison of isotropic projections of 2D (a-f) {^{23}Na}-^{1}H and (g,h) {^{27}Al}-^{1}H MQ-HETCOR (red) and MQ-SPAM-HETCOR (blue) spectra at ν_R = 62.5 kHz via (a,c,e,g) CP and (b,d,f,h) RINEPT. (a,b) NaH_2PO_4: NS = 24, RD = 1 s, 600 t_1 increments, T_{exp} = 4-6 h each. (c,d) Na_2HPO_4: NS = 24, RD = 1 s, 800 t_1 increments, T_{exp} = 5.5-8 h each. (e,f) Na citrate dihydrate: NS = 48, RD = 1 s, 600 t_1 increments, T_{exp} = 8-12 h each. (g,h) ipa-AlPO-14: NS = 96, RD = 0.6 s, 500 t_1 increments, T_{exp} = 8.3-12.3 h each.

Fig.**9** displays a series of {^{23}Na}-^{1}H and {^{27}Al}-^{1}H MQ-HETCOR and MQ-SPAM-HETCOR 2D spectra of the four samples via CPMAS and RINEPT transfers. It should be noted that the signal regions displayed in Fig.**9** occupy only a small part of the full spectra. This is related to the fact that the isotropic spectral width is proportional to ν_R, and hence is very large under fast MAS. The full spectra are shown in Fig.**S2** for NaH_2PO_4 and ipa-AlPO-14 and in Fig.**S3** for Na_2HPO_4 and Na citrate dihydrate.

The direct F2 dimension corresponds to the ^{1}H MAS spectra and the indirect F1 to the isotropic MQMAS spectra. For the ease of comparison, Fig.**10** shows the isotropic projections of the {^{23}Na}-^{1}H and {^{27}Al}-^{1}H MQ-HETCOR and MQ-SPAM-HETCOR 2D spectra of the four samples. In 2D experiments, the SPAM gains with CPMAS and RINEPT were found to be similar (i.e. slightly higher by 5%), to those observed in 1D (Fig.**8**).

V. Reduction of the experiment time

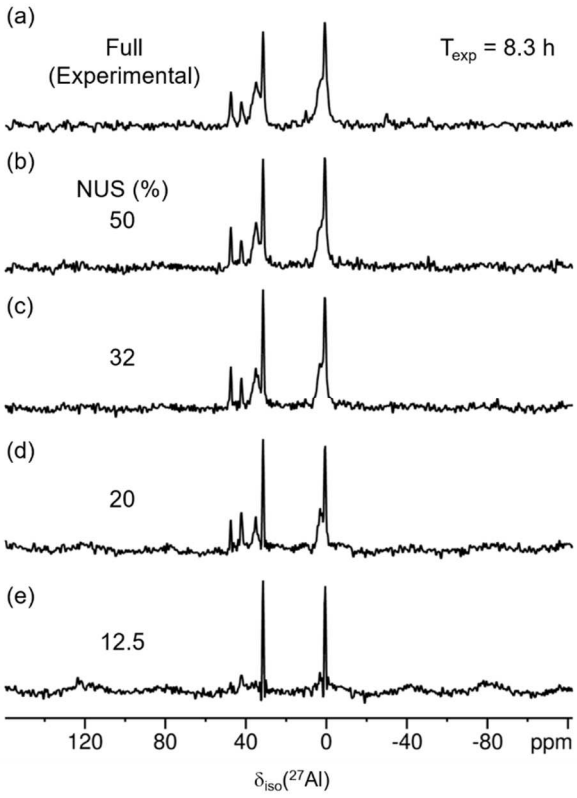

Fig.12 Comparison of isotropic projections of {^{27}Al}-^{1}H MQ-SPAM-CP-HETCOR spectra at ν_R = 62.5 kHz of ipa-AlPO-14: (a) Full (experimental) with NS = 96, RD = 0.6 s, 500 t_1 increments, T_{exp} = 8.3 h. (b) 50% NUS, (c) 32% NUS, (d) 24% NUS and (e) 12.5% NUS using the default random sampling scheme on TopSpin (i.e. no exponential weighting, NusT2 = 1 s) with the CS-IRLS algorithm (Mdd_mod = CS, Mdd_CsALG = IRLS) and the virtual echo option (Mdd_CsVE = TRUE) for processing

So far, the MQ-HETCOR and MQ-SPAM-HETCOR acquisitions of the four simple compounds presented in this study required 4-12 hours of the spectrometer time (Fig.**10**). One would then envisage to reduce T_{exp} of such long 2D acquisitions. We note here that our MQ-HETCOR and MQ-SPAM-HETCOR experiments are performed with "States" acquisition, with a minimum of scans per t_1 point due to the phase-cycling intrinsic to the pulse sequence: NS = 24 for I = 3/2 or 48 for I = 5/2. In our cases, the total duration has been related either (i) to this minimum phase cycling (NS = 24 for NaH_2PO_4), or (ii) to the limited sensitivity of the sample (NS = 96 for ipa-AlPO-14).

In the following, we briefly demonstrate the reduction of T_{exp} by two experimental tricks: the Echo-Antiecho acquisition for the case (i) and the non-uniform sampling (NUS) for the case (ii), respectively.

For I = 3/2 nuclei, on condition that the sensitivity is not a limiting factor, the "Echo-Antiecho" acquisition can be used to shorten the phase cycling with a minimum of NS = 12, as opposed to NS = 24 of the “States” acquisition. This reduces T_{exp} by a factor of 2. This time reduction can even be increased to 8/3 by using twice more echoes than anti-echoes (E:AE = 2:1).[39] Fig.**11** shows a comparison of the {^{23}Na}-^{1}H isotropic projections of the MQ-SPAM-HETCOR 2D spectra of NaH_2PO_4 and Na_2HPO_4 recorded with Echo-Antiecho acquisition. The information remains the same as with "States", but it was obtained in T_{exp} = 3 instead of 8 h. However, this time reduction also leads to a decrease of S/N, which is proportional to $\sqrt{T_{exp}}$, and hence it is only applicable to I = 3/2 systems with high S/N ratios.

For ^{27}Al (I = 5/2), the minimum NS of both MQ-HETCOR and MQ-SPAM-HETCOR is 48 with both Echo-Antiecho and “States” acquisitions. In this case, we can utilize a non-uniform sampling (NUS) along the indirect dimension to reduce T_{exp}. However, it should be remembered that this sampling can also be applied to I = 3/2 or any spin value. Fig.**12** shows a preliminary comparison of the isotropic projections of the {^{27}Al}-^{1}H MQ-SPAM-CP-HETCOR spectra of ipa-AlPO-14 upon NUS. Starting with the fully acquired 2D set of FIDs, NUS 2D sets with 50, 32, 24, and 12.5 % of t_1 points were obtained using the default random sampling scheme on TopSpin with the processing parameters in the free license. These different sets correspond to T_{exp} = 8.3, 4.15, 2.7, 1.7 and 1 h, with conventional acquisition, and NUS with 50, 33, 24 and 12.5 %, respectively. In this particular case of high-resolution spectra along the indirect dimension, down to 32, or even 24, % NUS may be safely employed, which thus lead to a great potential to reduce T_{exp} of such long 2D MQ-HETCOR experiments. We should, in principle, be able to improve the quality of our NUS MQ-HETCOR spectra by the use of more appropriate sampling schemes and/or processing algorithms,[42] which are currently under investigations.

VI. Conclusions

We have shown a comparison of the population transfers from the half-integer spin quadrupolar nuclei (^{23}Na or ^{27}Al) to ^{1}H via CPMAS and RINEPT in the context of MQ-HETCOR and MQ-SPAM-HETCOR under fast MAS conditions. Pros and cons of CPMAS and RINEPT transfers were discussed, and a step-by-

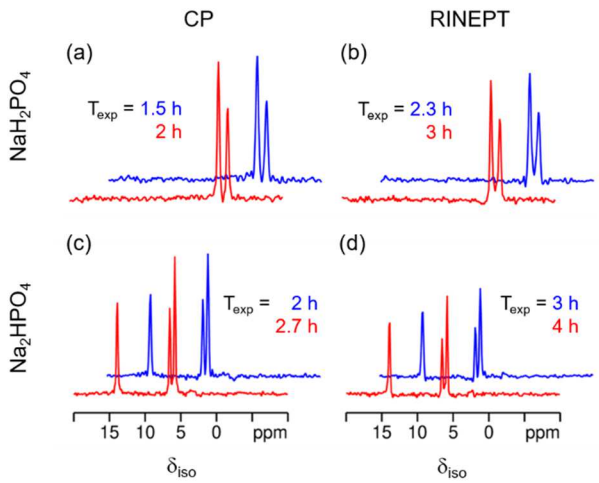

Fig.11 Comparison of isotropic projections of 2D {^{23}Na}-^{1}H MQ-SPAM-HETCOR spectra recorded by Echo-Antiecho acquisition with E:AE = 1:1 (red) and E:AE = 2:1 (blue), respectively, at ν_R = 62.5 kHz via (a,c) CP and (b,d) RINEPT. (a,b) NaH_2PO_4: NS = 12, RD = 1 s, 600 t_1 increments, T_{exp} = 2-3 h each. (c,d) Na_2HPO_4: NS = 24, RD = 1 s, 800 t_1 increments, T_{exp} = 2.7-4 h each.

step experimental setup procedure was established for the CPMAS, RINEPT and SPAM blocks with the aid of simulations and a series of 1D acquisitions. Due to the intrinsic MQMAS efficiency loss under fast MAS conditions, the SPAM sensitivity enhancement can be easily implemented to compromise the signal loss. Very recently, a very simple and efficient approach has been presented for 1Q ↔ 3Q transfers in the context of MQMAS experiments.[43] We believe that it is also a promising approach for MQ-HETCOR experiments, and it would be interesting to compare it with the SPAM approach.

We summarize the precautions to be used upon successful acquisition of the MQ-HETCOR signals via CPMAS and RINEPT. For CPMAS, use a very low rf-field on the quadrupolar channel (a few kHz) for the sake of efficient spin-locking. For RINEPT, carefully optimize the power input of the three CT-selective pulses on the quadrupolar channel (with an effective rf-field of a few kHz). The CPMAS efficiency is significantly affected by offsets or probe tuning instability, whereas RINEPT inevitably requires a ^{1}H presaturation period, which may result in a slightly longer experiment time than the CPMAS equivalent.

As a general conclusion, MQ-HETCOR experiments via CPMAS transfers are slightly more efficient (ca. 10-20 %) than with RINEPT using square π-pulses as basic element. However, CPMAS requires four parameters to optimize, instead of a single one with RINEPT: the recoupling time. This criterion is very important when the S/N is low. Moreover, it has been shown recently at ν_R = 62.5 kHz that the RINEPT and PRESTO-$R16_7^6$ transfers using ($270_0 90_{180}$) composite pulses are more efficient that with square π-pulses as basic element.[22] At ultra-fast MAS, these sequences are hence as efficient as CPMAS, and very simple to set due to their unique parameter to optimize. They are thus highly recommended to be used with MQ-HETCOR experiments.

Currently, we investigate several sampling schemes and/or processing algorithms for the non-uniform sampling (NUS) of the MQ-HETCOR acquisition. Furthermore, as a complementary approach,[11] ST-HETCOR is expected to exhibit much higher sensitivity under fast MAS and is also under investigations.

Conflicts of interest

There are no conflicts to declare.

Acknowledgements

The authors would like to thank Drs. Yu Tsutsumi and Hideaki Kimura (Bruker Japan K.K.) and Dr. Sebastian Wegner (Bruker BioSpin GmbH) for their help with the implementation of the pulse sequences on TopSpin software, and Dr. Wolfgang Bermel (Bruker BioSpin GmbH) for providing the AU programs.

References

1 L. Frydman and J. S. Harwood, *J. Am. Chem. Soc.*, 1995, **117**, 5367–5368.
2 Z. Gan, *J. Am. Chem. Soc.*, 2000, **122**, 3242–3243.
3 C. M. Morais, V. Montouillout, M. Deschamps, D. Iuga, F. Fayon, F. A. A. Paz, J. Rocha, C. Fernandez and D. Massiot, *Magn. Reson. Chem.*, 2009, **47**, 942–947.
4 A. Goldbourt, E. Vinogradov, G. Goobes and S. Vega, *J. Magn. Reson.*, 2004, **169**, 342–350.
5 S. H. Wang, S. M. De Paul and L. M. Bull, *J. Magn. Reson.*, 1997, **125**, 364–368.
6 S. Steuernagel, *Solid State Nucl. Magn. Reson.*, 1998, **11**, 197–201.
7 M. Roux, C. Marichal, J. L. Paillaud, C. Fernandez, C. Baerlocher and J. M. Chézeau, *J. Phys. Chem. B*, 2001, **105**, 9083–9092.
8 L. Delevoye, C. Fernandez, C. M. Morais, J. P. Amoureux, V. Montouillout and J. Rocha, *Solid State Nucl. Magn. Reson.*, 2002, **22**, 501–512.
9 C. Fernandez, C. Morais, J. Rocha and M. Pruski, *Solid State Nucl. Magn. Reson.*, 2002, **21**, 61–70.
10 J. W. Wiench, G. Tricot, L. Delevoye, J. Trebosc, J. Frye, L. Montagne, J. P. Amoureux and M. Pruski, *Phys. Chem. Chem. Phys.*, 2006, **8**, 144–150.
11 R. Siegel, J. Rocha and L. Mafra, *Chem. Phys. Lett.*, 2009, **470**, 337–341.
12 J. W. Wiench and M. Pruski, *Solid State Nucl. Magn. Reson.*, 2004, **26**, 51–55.
13 J. P. Amoureux, J. Trebosc, J. Wiench and M. Pruski, *J. Magn. Reson.*, 2007, **184**, 1–14.
14 S. E. Ashbrook, M. Cutajar, C. J. Pickard, R. I. Walton and S. Wimperis, *Phys. Chem. Chem. Phys.*, 2008, **10**, 5754–5764.
15 M. Castro, V. R. Seymour, D. Carnevale, J. M. Griffin, S. E. Ashbrook, P. A. Wright, D. C. Apperley, J. E. Parker, S. P. Thompson, A. Fecant and N. Bats, *J. Phys. Chem. C*, 2010, **114**, 12698–12710.
16 C. Martineau, B. Bouchevreau, F. Taulelle, J. Trébosc, O. Lafon and J. Paul Amoureux, *Phys. Chem. Chem. Phys.*, 2012, **14**, 7112–7119.
17 B. Bouchevreau, C. Martineau, C. Mellot-Draznieks, A. Tuel, M. R. Suchomel, J. Trébosc, O. Lafon, J. P. Amoureux and F. Taulelle, *Chem. Mater.*, 2013, **25**, 2227–2242.
18 B. Bouchevreau, C. Martineau, C. Mellot-Draznieks, A. Tuel, M. R. Suchomel, J. Trebosc, O. Lafon, J. P. Amoureux and F. Taulelle, *Chem. - A Eur. J.*, 2013, **19**, 5009–5013.
19 J. Trébosc, O. Lafon, B. Hu and J. P. Amoureux, *Chem. Phys. Lett.*, 2010, **496**, 201–207.
20 X. Zhao, W. Hoffbauer, J. S. auf der Günne and M. H. Levitt, *Solid State Nucl. Magn. Reson.*, 2004, **26**, 57–64.
21 R. Giovine, J. Trébosc, F. Pourpoint, O. Lafon and J. P. Amoureux, *J. Magn. Reson.*, 2019, **299**, 109–123.
22 J. S. Gómez, A. G. M. Rankin, J. Trébosc, F. Pourpoint, Y. Tsutsumi, H. Nagashima, O. Lafon and J.-P. Amoureux, *Magn. Reson.*, in press. https://doi.org/10.5194/mr-2021-29
23 J. Wack, R. Siegel, T. Ahnfeldt, N. Stock, L. Mafra and J. Senker, *J. Phys. Chem. C*, 2013, **117**, 19991–20001.
24 M. K. Pandey, H. Kato, Y. Ishii and Y. Nishiyama, *Phys. Chem. Chem. Phys.*, 2016, **18**, 6209–6216.
25 N. T. Duong and Y. Nishiyama, *Solid State Nucl. Magn. Reson.*, 2017, **84**, 83–88.
26 A. Venkatesh, M. P. Hanrahan and A. J. Rossini, *Solid State Nucl.*

Magn. Reson., 2017, **84**, 171–181.
27 A. Venkatesh, X. Luan, F. A. Perras, I. Hung, W. Huang and A. J. Rossini, *Phys. Chem. Chem. Phys.*, 2020, **22**, 20815–20828.
28 S. P. Brown, S. J. Heyes and S. Wimperis, *J. Magn. Reson. A*, 1996, **119**, 280–284.
29 J. P. Amoureux, C. Huguenard, F. Engelke and F. Taulelle, *Chem. Phys. Lett.*, 2002, **356**, 497–504.
30 M. Bak, J. T. Rasmussen and N. C. Nielsen, *J. Magn. Reson.*, 2000, **147**, 296–330.
31 A. J. Vega, *Solid State Nucl. Magn. Reson.*, 1992, **1**, 17–32.
32 J. Trebosc, B. Hu, J. P. Amoureux and Z. Gan, *J. Magn. Reson.*, 2007, **186**, 220–227.
33 A. Brinkmann and A. P. M. Kentgens, *J. Am. Chem. Soc.*, 2006, **128**, 14758–14759.
34 O. Lafon, Q. Wang, B. Hu, F. Vasconcelos, J. Trébosc, S. Cristol, F. Deng and J. P. Amoureux, *J. Phys. Chem. A*, 2009, **113**, 12864–12878.
35 Z. Gan and H. T. Kwak, *J. Magn. Reson.*, 2004, **168**, 346–351.
36 J. P. Amoureux, L. Delevoye, S. Steuernagel, Z. Gan, S. Ganapathy and L. Montagne, *J. Magn. Reson.*, 2005, **172**, 268–278.
37 P. K. Madhu, A. Goldbourt, L. Frydman and S. Vega, *Chem. Phys. Lett.*, 1999, **307**, 41–47.
38 A. P. M. Kentgens and R. Verhagen, *Chem. Phys. Lett.*, 1999, **300**, 435–443.
39 R. Siegel, T. T. Nakashima and R. E. Wasylishen, *Chem. Phys. Lett.*, 2005, **403**, 353–358.
40 A. Sasaki, Y. Tsutsumi and J. P. Amoureux, *Solid State Nucl. Magn. Reson.*, 2020, **108**, 101668.
41 J. P. Amoureux, M. Pruski, D. P. Lang and C. Fernandez, *J. Magn. Reson.*, 1998, **131**, 170–175.
42 K. Kazimierczuk, O. Lafon and P. Lesot, *Analyst*, 2014, **139**, 2702–2713.
43 I. Hung and Z. Gan, *J. Magn. Reson.*, 2021, **328**, 106994.

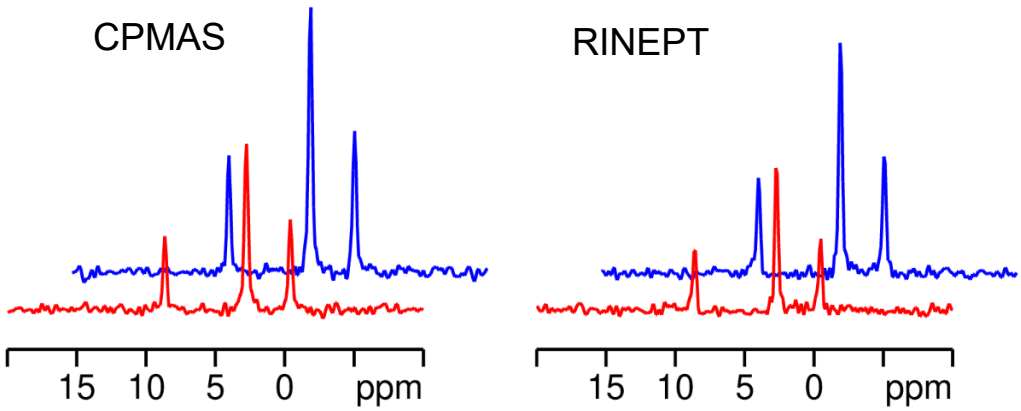

{^{23}Na}-^{1}H MQ-HETCOR (red) and MQ-SPAM-HETCOR (blue) ^{1}H spectra at ν_R = 62.5 kHz, with CPMAS (left) or RINEPT (right) transfer. CPMAS is slightly more efficient, but much more time-consuming to set-up.